Proceedings of 2023 IEEE
International Conference on Mechatronics and Automation
August 6 - 9, Harbin, Heilongjiang, China

Investigation of Aerodynamic Performance of Coaxial Rotors for Mars Rotorcraft

Pengyue Zhao*, Xifeng Gao, Zhenzhuo Yan, Yifan Li, Jianwei Wu and Zongquan Deng
Center of Ultra-Precision Optoelectronic Instrumentation Engineering
Harbin Institute of Technology
Harbin, China
pyzhao@hit.edu.cn, gaoxifeng123@163.com, billyjonas@163.com, 22B901027@stu.hit.edu.cn,
wujianwei@hit.edu.cn, zhaopengyue129@126.com

2023 IEEE International Conference on Mechatronics and Automation (ICMA) | 979-8-3503-2084-8/23/$31.00 ©2023 IEEE | DOI: 10.1109/ICMA57826.2023.10215711

***Abstract*—The coaxial rotor employed by NASA's Ingenuity helicopter is a typical configuration of the Martian rotorcraft, which requires different aerodynamic characteristics due to the particular physical properties of the Martian atmosphere. This work proposes a numerical model of coaxial rotors in the Martian atmosphere and uses computational fluid dynamics methods to perform numerical simulations. Hovering experiments are then used to verify the simulation results. The results indicate that the figure of merit and power loading of the coaxial rotor increase with the increase of the rotor separation distance, and the lower rotor produces less thrust than the upper rotor while consuming more power and thus has lower aerodynamic efficiency. The numerical simulation errors of rotor thrust and power are within 15%. Under the condition that the upper and lower rotor speeds are 2300 r/min and 2141 r/min, respectively, and the separation distance is 0.3R, the torque-balanced coaxial rotor system can carry 2.0 kg on Mars and requires a power of 166.4 W. The findings of this work provide a basis for the design of Mars coaxial rotorcraft.**

***Index Terms*—Martian rotorcraft, Coaxial rotor system, Aerodynamic performance, Experimental study, Numerical simulation**

I. Introduction

The Martian rotorcraft is a highly maneuverable aerial exploration platform that performs patrol and sampling missions on Mars. To improve its load capacity, various configurations such as coaxial, tandem, four-axis, and six-axis have been adopted [1]. Among them, the coaxial rotor configuration is particularly advantageous due to its compact structure and high power density [2]. In 2021, this configuration was chosen by NASA for the Ingenuity Helicopter, which was successfully deployed on the surface of Mars [3]. Furthermore, its potential for future Mars aircraft has been recognized by both NASA and JAXA [4], making the research on its aerodynamic performance in the Martian atmosphere highly significant.

Mars rotorcraft is significantly different from conventional Earth UAVs, which is mainly determined by Mars' special low Reynolds number near earth atmospheric environment [5]. In addition, the sand dust and unstable flow field on the surface of Mars also put forward strict requirements for the work of Mars rotorcraft. The characteristics of coaxial rotors in the terrestrial environment have been widely discussed. Leishman et al. proposed the BEMT to analyze coaxial rotors [6]. McAlister et al. developed the MSES code to predict AFDD coaxial rotor performance and study the effect of pitch angle and rotational speed on hovering performance [7]. Ramasamy conducted the hovering test of single and coaxial rotors to study the inflow interference between the upper and lower rotors [8]. Cameron et al. measure the hub loads of the hovering coaxial rotors [9]. However, there is limited research on the aerodynamic properties of coaxial rotors under Martian atmospheric conditions [10]. The low-temperature, low-density Martian atmosphere lowers the Reynolds number of the flow field in which the rotor resides, so the performance of the coaxial rotor on Mars differs from that on Earth [11]. The strong coupling between the flow fields of coaxial rotors makes the traditional blade element momentum theory unsuitable for calculating complex flow effects [12]. Therefore, the aerodynamic performance of the coaxial rotors in the Martian atmosphere needs to be analyzed through numerical simulation and hovering experiments. In addition, simulating the aerodynamic characteristics of Martian rotorcraft in the Martian atmosphere through ground experiments is crucial for verifying the accuracy of CFD simulation results.

This work utilizes computational fluid dynamics (CFD) to numerically simulate the aerodynamic characteristics of a coaxial rotor system in the Martian atmospheric environment. The hovering experiment was conducted in the Mars atmospheric environment simulator to verify the numerical simulation results and obtain the hovering properties of the coaxial rotors with different separation distances. The results presented in this paper provide insight into the impact of the structural parameters of the coaxial rotor system on its aerodynamic performance, thus improving the flight efficiency of the Mars coaxial rotorcraft.

II. Coaxial rotor system

The rotorcraft configuration for a Mars aircraft includes various types such as coaxial, tandem, ducted, and multi-axis configurations. Among these, the coaxial rotor system is particularly suitable due to its compact structure, lightweight design, and small rotor blade size, as well as its high propulsion and maneuverability efficiency. However, one drawback of this system is the complex flow field coupling effects between the coaxial rotors, which can result in a decline in aerodynamic performance. Therefore, it is essential to conduct

research on the coupled flow field between the coaxial rotors during their operation.

The schematic diagram of a coaxial rotor system is shown in Fig. 1. It comprises two rotors, an upper and a lower rotor, each with two blades of radius R = 0.5 m. The two rotors separated by a distance of H have the same rotational axis. The upper and lower rotors rotate at speeds of Ω_u and Ω_l, respectively, while their collective pitch angles are denoted by θ_u and θ_l, respectively. By adjusting these five parameters, the coaxial rotor system can achieve the highest hovering efficiency under certain loading constraints.

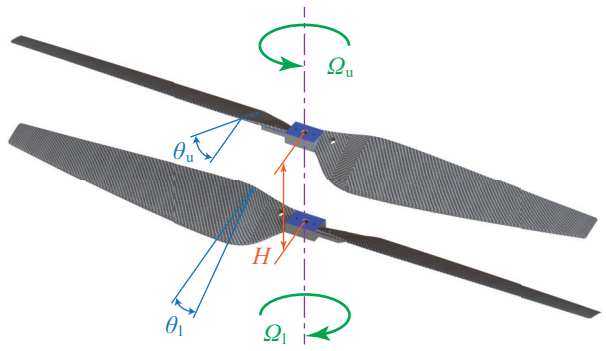

Fig. 1. Schematic diagram of the coaxial rotor system.

III. Methodology

A. Simulation conditions

The SST k–ω model is employed for numerical simulations performed in Ansys Fluent®, which has been proved suitable for low Reynolds number rotor simulations. The blade boundary and the outlet flow field boundary are selected as wall boundary conditions, while the inlet flow field boundary is set as a coupled boundary condition. The pressure at each boundary is set to 640 Pa, the temperature is set to 210 K, and the simulation parameters are consistent with the physical parameters of the Martian surface atmosphere.

The flow field meshing of the coaxial rotors is illustrated in Fig. 2. Fig. 2(a) shows the structured grid of the external flow field, and Fig. 2(b) displays the unstructured grid of the flow field around the rotors. The external flow field is in the geometry of a cylinder with a diameter of $6R$, while the distances from the upper or lower rotors to the top or bottom boundaries of the cylinder are $3R$ respectively, so as to reduce the wall effect of the aerodynamic simulation. The total height of the cylinder is determined by the distance H. The upper or lower rotor's surrounding flow fields are two cylinders with a diameter of $1.1R$ and a height of $0.8R$, which changes with the variation of the separation distance H.

B. Experimental condition

The split-type hovering performance test bench for the coaxial rotor, as demonstrated in Fig. 3. The coaxial rotor system adopts a split design, and the coaxiality of the rotor system exceeds 5mm. Both of the rotor systems are independently

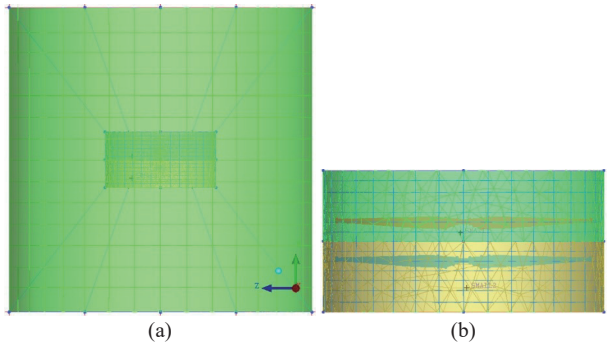

Fig. 2. Flow field meshing for numerical simulation. (a) Structured grid of the external flow field, (b) Unstructured grid of surrounding flow field.

driven to avoid transmission coupling. The drive motors of the upper and lower rotors are equipped with speed sensors to measure the speed of the upper and lower rotors. The upper and lower rotor bases are equipped with S-shaped sensors and torque sensors, respectively used to measure the thrust and torque generated by the rotor. The distance adjustment module below the lower measurement module adjusts the separation distance between the two rotors, and the base of the module can adjust the lower rotor axis to meet the coaxial requirements of the rotor system.

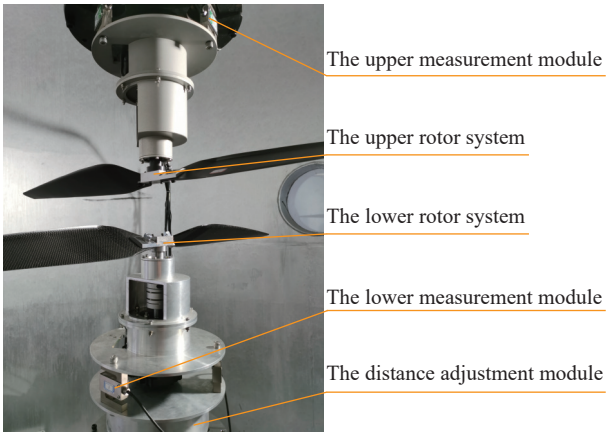

Fig. 3. Split-type hovering performance test bench for the coaxial rotor system.

The coaxial rotor hovering performance experiment is conducted in a Martian atmospheric environment simulator, where the gas pressure is adjusted to obtain the density of the Martian atmosphere. The experiment employs trapezoidal low Reynolds number blades manufactured with 3D-printed carbon fiber materials. The rotor configuration and test conditions used in the hovering experiments are listed in Table I.

The simulation verification experiments are conducted to evaluate the aerodynamic simulation results of the coaxial rotor system. In these experiments, the rotor speed is set to 2300 r/min, and the separation distance is varied from 100 to 600 mm. Additionally, a torque matching experiment is performed to investigate the conditions for achieving a

TABLE I
ROTOR CONFIGURATION AND TEST CONDITIONS IN HOVERING EXPERIMENTS

Item	Parameters
Airfoil	NACA 6904
Rotor diameter (mm)	1000
Blade chord length (mm)	70
Blade twist angle (°)	–10
Rotor speed range (r/min)	1000–3000
Separation distance range (mm)	50–600

resultant torque of zero. This experiment fixes the upper rotor speed at 2300 r/min and the separation distance at 150 mm. At this point, adjust the lower rotor speed of the coaxial rotor system until the speed range of the lower rotor covers the corresponding speed at the moment of torque balance.

IV. RESULTS

A. Numerical simulation

Fig. 4 illustrates the effect of the separation distance on the thrust and power generated by the rotor system. It is found that, with the increase of the separation distance, the thrust and the required power of both the rotor systems are continuously increasing at the same speed. And the rate of this increase trend gradually decreases. The thrust and power curves' slope become smaller as the separation distance increases, indicating that there is only weak inflow disturbance between the coaxial rotors when the separation distance is more than $0.6R$. With the same rotational speed, the upper rotor generates greater thrust than the lower rotor, due to its higher induced speed. The lower rotor requires more hover power than the upper one, which is caused by the eddy current loss of the blade tip.

By normalizing the thrust and power generated by the coaxial rotor system, the thrust coefficient C_{T} and power coefficient C_{P} can be expressed as in Eq. 1.

$$\begin{cases} C_{\mathrm{T}} = \dfrac{T}{\rho A \Omega^2 R^2} \\ C_{\mathrm{P}} = \dfrac{P}{\rho A \Omega^3 R^3} \end{cases} \tag{1}$$

where A is the aera of the blade disk and ρ is the ambient gas density. The curves of C_{T} and C_{P} are illustrated in Fig. 5, the law of which is consistent with the curves in Fig. 4. Based on this, the hovering performance evaluation index of the rotor system can be derived.

The hovering efficiency of the coaxial rotors can be evaluated using the power loading PL and figure of merit FM. The figure of merit is typically characterized by the ratio of the 1.5 square of the thrust generated by the rotor system in a stable hovering state to the power consumed at that time, i.e. $FM = {C_{\mathrm{T}}}^{3/2} \Big/ \sqrt{2} C_{\mathrm{P}}$. The FM curves of the coaxial rotors with different separation distances are shown in Fig. 6. The power loading is the ratio of rotor thrust to the power required and its curves are depicted in Fig. 7.

Fig. 6 shows that the figure of merit of the two rotors and coaxial system all increase with the separation distance.

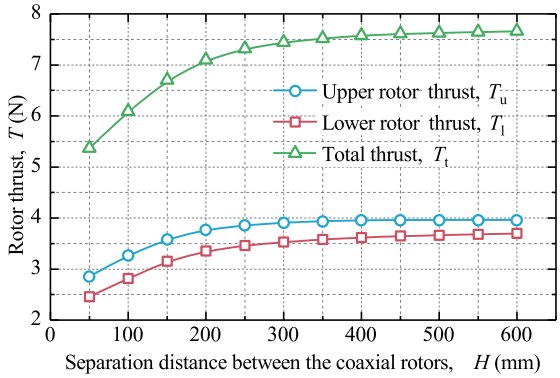

(a) The variation of rotor thrust vs. separation distance between the upper and lower rotors

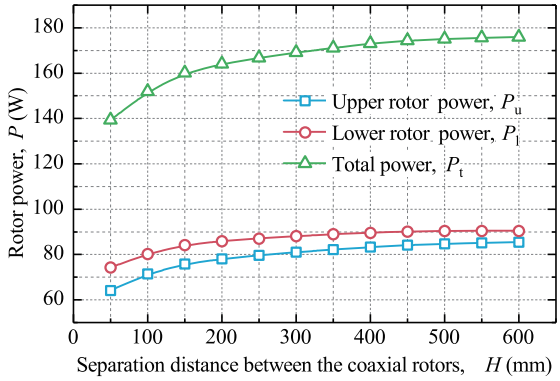

(b) The variation of rotor power vs. separation distance between the upper and lower rotors

Fig. 4. The variations of rotor thrust and power vs. separation distance between the upper and lower rotors.

The upper rotor is more aerodynamically efficient than the lower one due to the aerodynamic coupling effect. When the separation distance exceeds $0.6R$, the aerodynamic coupling effect between the rotors is weakened, and the aerodynamic efficiency is no longer improved. Fig. 7 illustrates that at a fixed separation distance, the power loading of the upper rotor is larger than that of the coaxial rotor system as well as the lower rotor, indicating that the main load capacity of the coaxial system comes from the upper rotor. Therefore, in the torque matching experiment, the flight parameters of the upper rotor are fixed, while the flight parameters of the lower rotor are adjusted.

The thrust conversion efficiency is the ratio of the average thrust generated by the coaxial rotors to that of a single rotor, as displayed in Fig. 8. Similarly, the power conversion efficiency is the ratio of the average power of the coaxial rotors to the power of a single one, as shown in Fig. 9. Both of these ratios can be expressed as $(T_{\mathrm{u}} + T_{\mathrm{l}})/(2\,T_0)$ and $(P_{\mathrm{u}} + P_{\mathrm{l}})/(2\,P_0)$, respectively.

Figs. 8 and 9 reveal that both the thrust and power conversion efficiency increase with the increase of the separation distance H, but the increase gradually slows down. When H is equal to $0.3R$, $(T_{\mathrm{u}} + T_{\mathrm{l}})/(2\,T_0)$ is 0.8 and $(P_{\mathrm{u}} + P_{\mathrm{l}})/(2\,P_0)$ is 0.85. When H increases to $0.6R$, neither $(T_{\mathrm{u}} + T_{\mathrm{l}})/(2\,T_0)$

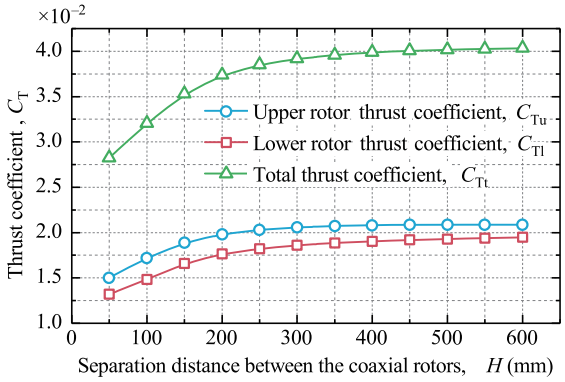

(a) The variation of thrust coefficient vs. separation distance between the upper and lower rotors

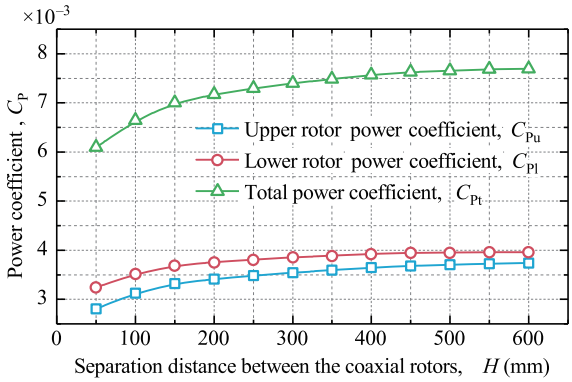

(b) The variation of power coefficient vs. separation distance between the upper and lower rotors

Fig. 5. The variation patterns of thrust and power efficiency of coaxial rotor systems under different separation distance conditions.

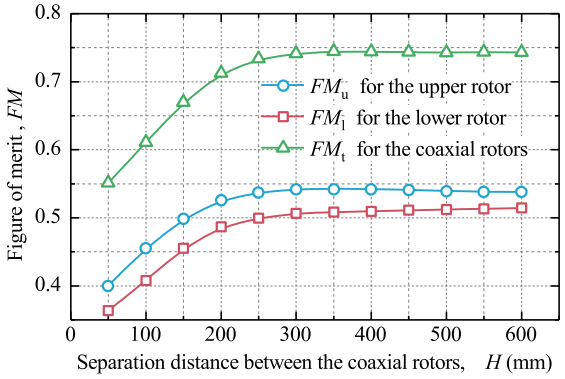

Fig. 6. The variation curve of the figure of merit of the rotor system as the separation distance changes.

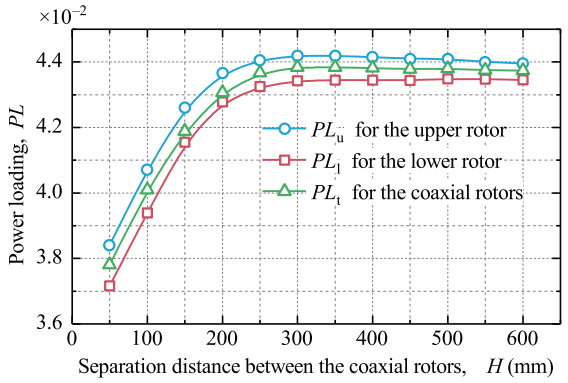

Fig. 7. The variation curve of the power loading of the rotor system as the separation distance changes.

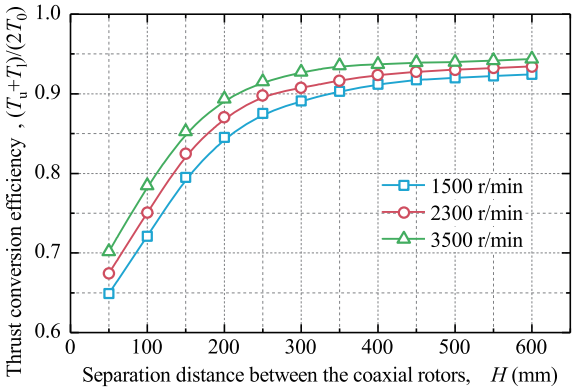

Fig. 8. The variation pattern of thrust conversion efficiency in coaxial rotor systems under different separation distance conditions.

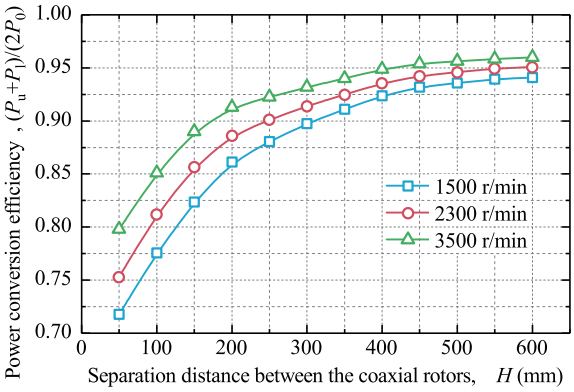

Fig. 9. The variation pattern of power conversion efficiency in coaxial rotor systems under different separation distance conditions.

nor $(P_u + P_l)/(2P_0)$ is less than 0.9. Both $(T_u + T_l)/(2T_0)$ and $(P_u + P_l)/(2P_0)$ increase with the increase of rotor speed Ω.

B. Simulation verification

Figs. 10 and 11 conducted experimental verification on the CFD simulation results of the thrust and power generated by the rotor system under the condition of Martian atmospheric density. It is observed that the experimental results are higher than the numerical simulation values. Nevertheless, the curves consistently reveal that the thrust of the upper rotor is higher than that of the lower one with the same separation distance, while the power of the upper rotor is lower than that of the lower rotor.

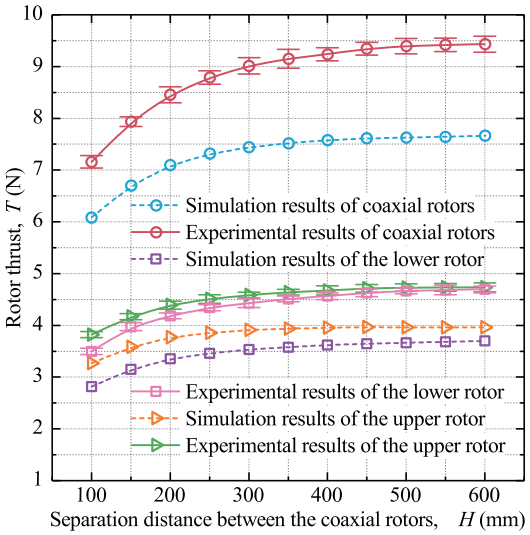

Fig. 10. Experimental verification of CFD simulation results for rotor system thrust.

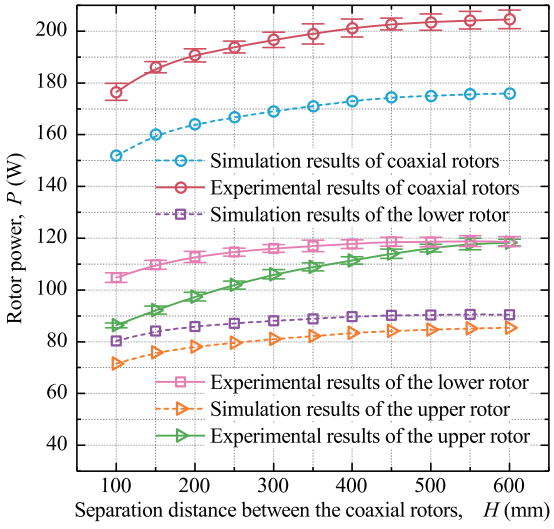

Fig. 11. Experimental verification of CFD simulation results for rotor system required power.

The error of the numerical simulation results increases with the rotor separation distance. The maximum error of rotor thrust and power is less than 15%. This error is due to the limitations of the SST k–ω model used in the numerical simulation, which is unable to accurately capture the mixed flow field of laminar and turbulent flow in a low Reynolds number condition. It is very meaningful to carry out Mars low Reynolds number simulation. Because it requires a lot of time and cost to carry out the ground verification experiment of Mars rotorcraft, the aerodynamic characteristics of the airfoil and blade structure of Mars rotorcraft will be analyzed first by using the simulation method, and the aerodynamic structure suitable for the Martian atmospheric environment will be optimized, which will greatly improve the development efficiency of Mars rotorcraft.

C. Torque matching

Due to the coupled flow field generated by the coaxial rotor system and the inconsistent degree of coupling between the upper and lower rotors, when the upper and lower rotors have the same rotational speed, the entire rotor system will have a torque that cannot be completely canceled out. This will make it difficult for the rotor system to hover stably, so it is necessary to carry out torque matching tests for the coaxial rotor system. Torque matching aims to control the resultant torque of the coaxial rotor to zero. The lower rotor speed is adjusted under the constraints from Section III-B. Fig. 12 illustrates the torque generated by the two rotors as a function of the lower rotor speed. By matching the torques, the resultant torque can be controlled to zero. At this point, the rotor system will only generate thrust and not rotate due to torque.

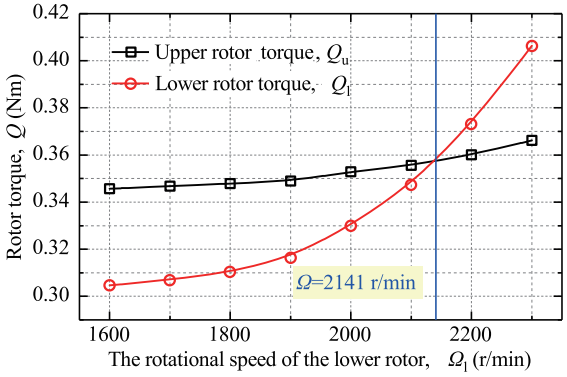

Fig. 12. The torque matching experiment of the coaxial rotor system changes with the speed of the lower rotor system.

The coaxial rotor system is torque balanced when the upper rotor is spinning at 2300 r/min as well as the lower rotor is spinning at 2141 r/min. As the lower rotor speed increases, the torque generated by the upper rotor at a fixed speed increases due to the increased lower rotor inflow, which in turn increases the induced speed of the upper rotor plane. During the torque matching experiment, the thrust and power curves are shown in Fig. 13.

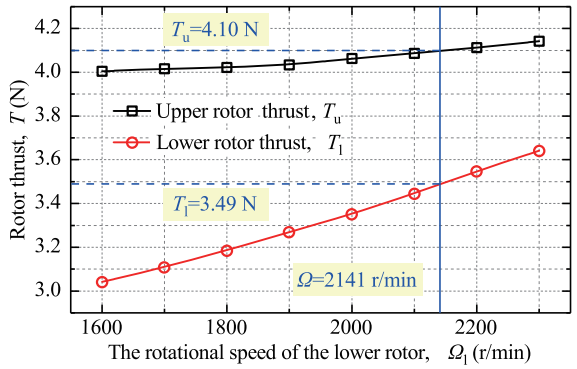

(a) The variation of rotor thrust vs. rotational speed of the lower rotor

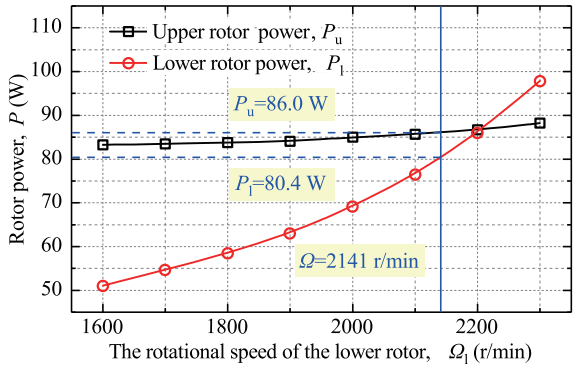

(b) The variation of rotor power vs. rotational speed of the lower rotor

Fig. 13. Experimental results of torque matching for coaxial rotor systems.

It was found that under the condition of torque matching in the coaxial rotor system, the rotor system of the Martian rotorcraft can generate 7.59 N of thrust, with a corresponding power loss of 166.4 W. Based on the fact that the Martian gravity acceleration is about 3/8 of the Earth's gravity acceleration, this rotor system can support unmanned aerial vehicles with a mass of 2.0 kg working in Martian environments. Note that considering that Mars rovers can only load limited mass components, it is necessary to strictly limit the quality of Mars rovercraft. Based on the complex requirements of Mars rovers, this work mainly focuses on the rotor system of Mars rotorcraft with a mass of 2.0 kg.

V. Conclusion

The Martian rotorcraft is a highly maneuverable aerial exploration platform that performs patrol and sampling missions on Mars. To improve its load capacity and various configurations, this work presents numerical simulations and experiments of coaxial rotors in the Martian atmosphere to investigate the aerodynamic performance of the rotor system. Results show that the thrust and power of the coaxial rotors increase with the separation distance between the rotors, with the upper rotor generating more thrust than the lower rotor and requiring less power. The figure of merit and power loading of both rotors also increase with the separation distance, with the upper rotor having higher aerodynamic efficiency. The numerical simulations of rotor thrust and power are found to be lower than the experimental results, with an error of less than 15%. A torque balance was achieved under the condition of an upper rotor speed of 2300 r/min, a lower rotor speed of 2141 r/min, and a separation distance of $0.3R$. Experiments reveal that the torque-matched coaxial rotor system can carry 2.0 kg on Mars and requires a power of 166.4 W. The findings of this work provide a basis for the design of Mars coaxial rotorcraft. Besides, this work provides a decoupling measurement method for the hovering lift drag characteristics of coaxial rotor systems. Based on CFD simulation and experimental results analysis, it can effectively evaluate whether the thrust generated by the coaxial rotor system is sufficient and whether the power loss of the rotor is feasible.

Acknowledgment

This work was supported by the National Natural Science Foundation of China (52105547), the China Postdoctoral Science Foundation (2021M700995), the Natural Science Foundation of Heilongjiang Province, China (LBH-Z21063), and the Young Elite Scientists Sponsorship Program by CAST (2022QNRC001).

References

[1] D. Escobar, I. Chopra, and A. Datta, "High-fidelity aeromechanical analysis of coaxial mars helicopter," *Journal of Aircraft*, vol. 58, no. 3, pp. 609–623, 2021.

[2] S. Cappucci, M. T. Pauken, J. A. Moulton, and D. W. Hengeveld, "Assessment of the mars helicopter thermal design sensitivities using the veritrek software," 2018.

[3] J. Balaram, M. Aung, and M. P. Golombek, "The ingenuity helicopter on the perseverance rover," *Space Science Reviews*, vol. 217, no. 4, p. 56, 2021.

[4] B. T. Pipenberg, S. A. Langberg, J. D. Tyler, and M. T. Keennon, "Conceptual design of a Mars rotorcraft for future sample fetch missions," in *2022 IEEE Aerospace Conference (AERO)*. IEEE, 2022, pp. 01–14.

[5] B. T. Pipenberg, M. Keennon, J. Tyler, B. Hibbs, S. Langberg, J. Balaram, H. F. Grip, and J. Pempejian, "Design and fabrication of the mars helicopter rotor, airframe, and landing gear systems," in *AIAA Scitech 2019 Forum*, 2019, p. 0620.

[6] M. Syal and J. G. Leishman, "Aerodynamic optimization study of a coaxial rotor in hovering flight," *Journal of the American Helicopter Society*, vol. 57, no. 4, pp. 1–15, 2012.

[7] J. W. Lim, K. W. McAlister, and W. Johnson, "Hover performance correlation for full-scale and model-scale coaxial rotors," *Journal of the American Helicopter Society*, vol. 54, no. 3, pp. 32 005–32 005, 2009.

[8] M. Ramasamy, "Hover performance measurements toward understanding aerodynamic interference in coaxial, tandem, and tilt rotors," *Journal of the American Helicopter Society*, vol. 60, no. 3, pp. 1–17, 2015.

[9] C. G. Cameron, J. Sirohi, and D. Uehara, "Transient hub loads and blade deformation of a mach-scale coaxial rotor in hover," in *56th AIAA/ASCE/AHS/ASC Structures, Structural Dynamics, and Materials Conference*, 2015, p. 1412.

[10] H. F. Grip, D. Conway, J. Lam, N. Williams, M. P. Golombek, R. Brockers, M. Mischna, and M. R. Cacan, "Flying a helicopter on Mars: How Ingenuity's flights were planned, executed, and analyzed," in *2022 IEEE Aerospace Conference (AERO)*. IEEE, 2022, pp. 1–17.

[11] W. J. Koning, W. Johnson, and H. F. Grip, "Improved Mars helicopter aerodynamic rotor model for comprehensive analyses," *AIAA Journal*, vol. 57, no. 9, pp. 3969–3979, 2019.

[12] H. F. Grip, J. Lam, D. S. Bayard, D. T. Conway, G. Singh, R. Brockers, J. H. Delaune, L. H. Matthies, C. Malpica, T. L. Brown *et al.*, "Flight control system for nasa's mars helicopter," in *AIAA Scitech 2019 Forum*, 2019, p. 1289.